FISHERIES OCEANOGRAPHY

FISHERIES OCEANOGRAPHY Fish. Oceanogr. 24:1, 69–89, 2015

Do *Sardinella aurita* spawning seasons match local retention patterns in the Senegalese–Mauritanian upwelling region?

BAYE CHEIKH MBAYE,[1,2,*] TIMOTHÉE BROCHIER,[3] VINCENT ECHEVIN,[2] ALBAN LAZAR,[2] MARINA LÉVY,[2] EVAN MASON,[4] AMADOU THIERNO GAYE[1] AND ERIC MACHU[5]

[1]*Laboratoire de Physique de l'Atmosphère et de l'Océan Siméon Fongang (LPAO-SF), ESP/UCAD, BP 5085, Dakar-Fann, Senegal*

[2]*LOCEAN-IPSL, CNRS/IRD/UPMC, Boîte 100 – 4, Place Jussieu, 75252, Paris Cedex 05, France*

[3]*Institut de Recherche pour le Développement (IRD), LEMAR/CRODT, BP 1386, Dakar, Sénégal*

[4]*Mediterranean Institute for Advanced Studies, IMEDEA (UIB-CSIC), Esporles, IMEDEA - C/ Miquel Marqués, 21 - 07190 Esporles, Esporles - Illes Balears, Spain*

[5]*Laboratoire de Physique des Océans (LPO), Institut de Recherche pour le Développement (IRD), BP 70, 29280, Plouzané, France*

ABSTRACT

Sardinella aurita is the most abundant small pelagic fish in the Senegalese–Mauritanian region. The success of its reproduction crucially depends on the local circulation as this determines whether larvae reach coastal nursery areas favorable to their survival or are dispersed into the open ocean. As a first step towards evaluating sardinella vulnerability to climate-driven hydrodynamical changes, this study aims at underpinning how transport pathways drive optimal spatial and seasonal patterns for sardinella reproduction. We have used two estimates of the Senegalese–Mauritanian coastal seasonal circulation simulated by two hydrodynamical model configurations that differ in their forcing and topography. Nursery areas are determined by evaluating coastal retention with a Lagrangian individual-based model that accounts for processes such as diel vertical migration and mortality as a result of lethal temperature exposure. Our results suggest that the shelf zones located at the Arguin Bank (19.5°N–21°N) and south of Senegal (12°N–14.75°N) are highly retentive. We find maximum retention rates in July–August and November–December over the Arguin Bank; from February–July and November–December over the southern Senegalese shelf; and lower retention rates over the central region (14.75°N–19.5°N) that are locally maximum in June–July when the upwelling weakens. These retention areas and their seasonality are in agreement with previously reported spawning patterns, suggesting that the *Sardinella aurita* spawning strategy may result from a trade-off between retention patterns associated with the seasonal circulation and food availability. Exposure to lethal temperatures, although not well studied, could be a further limiting factor for spawning. The Lagrangian analysis reveals important connectivity between sub-regions within and south of the system and hence underlines the importance for joint management of the *Sardinella aurita* stock.

Key words: bio-physical model, canary current system, connectivity, larval retention, recruitment, *Sardinella aurita*, Senegalese–Mauritanian upwelling, spawning

INTRODUCTION

Within the Canary Current System (CCS), the Senegalese–Mauritanian region is one of the most productive owing to its wide shelf and strong seasonal upwelling with maximum intensity from winter to spring (Wooster *et al.*, 1976; Van Camp *et al.*, 1991; Roy, 1992; Demarcq, 1998). The west African *Sardinella aurita* is the dominant small-pelagic fish species in this region. It is intensively exploited and crucial to the economies of the West African countries. Indeed, *Sardinella aurita* is the primary species fished in Senegal, and the second in Mauritania, with total landings exceeding 500 000 tons per year (Corten *et al.*, 2012; FAO, 2012). The key role of sardinella in the CCS marine ecosystem (Cury *et al.*, 2000) underlines the need to expand our knowledge regarding this species.

Sardinella aurita recruitment, as for other small pelagic fish, is highly variable and relies on variability of the coastal upwelling intensity (Bakun, 1996; Lett *et al.*, 2006) and the associated variations in phytoplankton productivity (Arístegui *et al.*, 2006; Fréon

*Correspondence. e-mail: bayecheikha@hotmail.fr

Received 13 December 2013
Revised version accepted 17 November 2014

et al., 2006). Over-fishing, through the truncation effect of the population age structure, might further increase the level of dependence of stock size on environmental variability (Perry *et al.*, 2010).

The recruitment of *Sardinella aurita*, like most clupeoids, mostly depends upon survival during the early stages of its life cycle: pelagic eggs and larvae are passively transported by ocean currents, which may carry them either to plankton-rich coastal areas representing favorable nurseries or to the open ocean where they are exposed to starvation and predation. Understanding the subtle balance in environmental conditions required for *Sardinella aurita* larval survival is necessary to assess the vulnerability of this species to changes related to natural and anthropogenic climate variability (e.g., Lasker, 1975, 1978).

Because of the spatial variability and strong seasonality of the coastal upwelling, *Sardinella aurita* spawning is not uniform along the coast but occurs preferentially over the Arguin Bank (Mauritania), to the south of Cap-Vert (Senegal) (Fig. 1; Conand, 1977; Boely *et al.*, 1978, 1982) and, to a lesser extent, in-between the two regions (Fréon, 1988). Over the Arguin Bank, spawning occurs in July–August during the minimum of the upwelling season and in November–December which corresponds to the onset of peak upwelling (Boely *et al.*, 1982; Taleb, 2005; Lathuilière *et al.*, 2008). South of Senegal, spawning peaks during the upwelling season (February–June), and at the end of summer when the upwelling shuts down for a couple of months (September–November) (Boely, 1979; Boely *et al.*, 1982; Fréon, 1988). In between these two regions (southern Mauritania and northern Senegal), spawning is maximum in June–July (Fréon, 1988).

Figure 1. SeaWIFs Surface chlorophyll-a concentration annual mean (mg Chl m^{-3}), over the period 1997–2006. Black contour marks the 200-m isobath. Hatched areas correspond to observed spawning locations (adapted from Boely *et al.*, 1982).

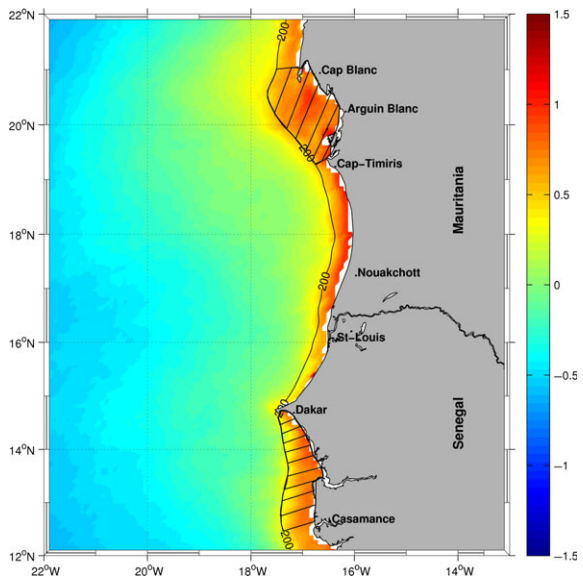

It has been hypothesized that small pelagic fish adapt their spawning strategy to the specificities of their environment in order to optimize larval survival (Lasker, 1975; Cury and Roy, 1989; Bakun, 1996; Cury *et al.*, 2008). In this study, we test the importance of retention of sardinella eggs and young larvae within their spawning areas using an individual-based Lagrangian model of larval transport. Suitable spawning areas are considered to be the continental shelf delimited from the coast to the 200-m isobath, which is within the chlorophyll-rich coastal band (Fig. 1) where larvae can survive while drifting. Considering a narrow band is meaningful as spawning always occurs over the continental shelf and more probably in its coastal part (Conand, 1977; Boely *et al.*, 1982). The modeled retention patterns are then compared with observed spawning patterns. This approach also allows us to study larval connectivity along the coast. Understanding connectivity pathways is necessary for the joint management of *Sardinella aurita* populations that overlap the exclusive economic zones of several countries in the region.

Similar approaches have been conducted in the Iberian (Santos *et al.*, 2005; Marta-Almeida *et al.*, 2006; Peliz *et al.*, 2007) and Moroccan (Brochier. *et al.*, 2008b) nearshore regions of the CCS. Recently, Dias *et al.* (2014) investigated the spawning strategies and larval survival of the Brazilian Sardine in the South Brazil Bight. To our knowledge, the present study is the first one based on Lagrangian modeling focusing on the Senegal–Mauritanian coastal regions in the southern part of the CCS.

METHODOLOGY

In order to explore whether larval coastal retention patterns can explain *Sardinella aurita* spawning strategies, retention patterns are estimated using an individual-based Lagrangian model of larval transport, forced with circulation fields derived from two different regional hydrodynamic models. Using two evaluations of the circulation enables us to enhance the robustness of our results.

Hydrodynamical modeling

The Regional Oceanic Modeling System (ROMS) (Shchepetkin and McWilliams, 2005) is used to

simulate temperature fields and three-dimensional currents. It solves the Primitive Equations in an Earth-centered rotating environment, based on the Boussinesq approximation and hydrostatic vertical momentum balance. ROMS is discretized in terrain-following curvilinear coordinates. For more details on the model parameterizations, the reader is referred to Shchepetkin and McWilliams (2005). The model grids, atmospheric forcing, initial and boundary conditions were built using the ROMSTOOLS (Penven *et al.*, 2008) and roms2roms (Mason *et al.*, 2010) toolboxes.

Two different model configurations were used. The first experiment (SM1) encompasses the entire CCS from 5°N to 41°N and from 30°W to 5°W at a horizontal resolution of 1/4° and 32 vertical levels (Machu *et al.*, 2009). A child grid at 1/12° (~8.3 km) is embedded over the Senegalese–Mauritanian domain using the AGRIF software (Debreu *et al.*, 2012). The bottom topography originates from GEBCO 1' data base (http://www.gebco.net) . The minimum depth of ROMS bottom topography at the coast reaches 50 m.

In this study we focused on the seasonal cycle, leaving aside the interannual variability. The model (coarse and fine grids) was forced with the COADS (Da Silva *et al.*, 1994) surface monthly climatology of heat and fresh water fluxes, and by a 1/2° wind stress monthly climatology derived from QuikSCAT satellite scatterometer (Liu *et al.*, 1998). The three lateral open boundaries of the coarse grid were forced using a climatology of temperature, salinity and derived geostrophic velocity from the World Ocean Atlas Data (WOA2001) (Conkright *et al.*, 2002), and the fine grid open boundaries were forced at each time step by the coarse grid solution.

A second experiment (SM2) was used to test the robustness of the results obtained with SM1. Outputs from the CCS ROMS model configuration (at 7.5 km resolution) used by Mason *et al.* (2011) were extracted for the Senegalese–Mauritanian region. The topography of SM2 was different from SM1, where the ETOPO2 data base (Smith and Sandwell, 1997) at 2' × 2' spatial resolution is used with shallower shelves (minimum depth of 15 m at the coast; Fig. 8) and a topographic hole in the Arguin Bank (Fig. 4). The 1/4° SCOW (Scatterometer Climatology of Ocean Winds, based on Quikscat data) climatological wind stress product was used to force SM2 (Risien and Chelton, 2008). Details of the settings and evaluation of the SM2 simulation can be found in Mason *et al.* (2011). In SM1 and SM2, the model SST is restored towards Version 4 of the Pathfinder SST (Kilpatrick *et al.*, 2001) according to the parameterization of Barnier *et al.* (1995).

Table 1. Description of the main parameters of the hydrological and Lagrangian experiments.

Model configurations	SM1/SM2
Spatial resolution	8.3/7.5 km
Wind forcing	Quikscat (1/2°)/SCOW climatology (1/4°)
Number of simulated years	6
Time-average of hydro dynamical model output	2/3 days
Release date (t_0)	Each month
Release area	Continental shelf (200 m-isobath)
Depth range of spawning	0–20 m
Passive phase (from t_0 to t_1)	8 days
Diurnal Vertical Migration (DVM) range (from 8 to 28 days)	20, 30, 60, 100, none (PT)
Lethal temperature tresholds	14, 16, 18°C
Ichthyop model time step	2 h

The two model solutions have a spin-up phase of 4 years, after which statistical equilibrium of the dynamics is reached (Figures not shown). The following 6 years of the respective simulations are used for our analyzes. Model outputs were saved every 2 days and every 3 days for SM1 and SM2, respectively (Table 1).

Individual-based Lagrangian model

ICHTHYOP (http://www.ichthyop.org/) is used to simulate larval transport. This tool is designed to study the effects of physical and biological factors on ichthyoplankton dynamics. For a complete description of the model, the reader is referred to Lett *et al.* (2008) and Brochier *et al.* (2008a). The Lagrangian model allows us to explore a small range of larval behaviors and vulnerabilities (e.g., diel vertical migration and impact of lethal temperature). Larval mortality is considered to occur when eggs and larvae are exposed to temperatures below a pre-defined threshold value. We did not find information about lethal temperature in the Senegalese–Mauritanian region, but field measurements show that *Sardinella aurita* larvae are found between 18 and 30°C (Conand, 1977). Thus, the impact of cold lethal temperatures is tested (14, 16 and 18°C). The model also simulates larval vertical swimming behavior in the form of diurnal vertical migration (DVM) between the surface and a fixed depth. Measurements show that *Sardinella aurita* eggs are concentrated in the surface mixed layer over the continental shelf (Matsuura, 1971). As the mixed-layer base is particularly shallow in the region of interest (between 10 and 30 m; De Boyer Montégut *et al.*, 2004), and given the

lack of observations of diel migration, we tested a set of four DVM depths: 20, 30 m (within the mixed layer), 60 and 100 m (below the mixed layer depth), hereinafter DVM20, DVM30, DVM60 and DVM100, respectively. Sardinella larvae are nearly absent at depths >60 m (Conand, 1977); consequently, DVM60 and mainly DVM100 were included as hypothetical experiments to test the limits of the model. A simple experiment (hereafter PT for passive transport) was also performed where no DVM is included such that larvae are passively transported. *Sardinella aurita* larvae samples off Brazil have shown that the formation of a swim bladder, which is essential for the larvae to remain at specific depths, appears at an age of ~7 days (Ditty *et al.*, 1994). As such information is not known in the Senegalese–Mauritanian region, we tested the impact of swim-bladder development age of 6, 7, 8 and 9 days and found similar results, thus an intermediate value of 8 days was chosen. Before hatching, eggs float at the surface. The larvae are considered to be passive particles that follow water parcels between hatching and 8 days. We used a hatching time of 1 day (Matsuura, 1975; Conand, 1977). After 8 days, larvae begin DVM and spend half of their time at the surface (during the night) and half of their time at the DVM depth to escape predation (during the day).

We use a fourth order Runge Kutta advection scheme with a time step of 2 h to simulate the transport of particles forced by 2-day averaged (three day averaged) velocities from the SM1 (SM2) solution. Sensitivity tests show that the particle trajectories are very similar with velocities averaged at a higher frequency (up to 4 h), indicating a weak contribution of inertia-gravity waves to transport at the scales considered.

Release experiments

We conducted a set of experiments where 10 000 virtual eggs were homogeneously released over the shelf (defined as the region between the coast and the 200 m isobath) from 12°N to 21°N (Fig. 1). The eggs were released at the beginning of each month randomly between the surface and 20 m depth over the entire region, no seasonal spawning pattern being assumed *a priori*.

The survival rate of each cohort was evaluated after 28 days of transport. Transformation to juvenile is complete at a size of ~23 mm, which is reached in ~27.2 days for a larval growth rate of 1.2 mm day^{-1} (Ditty *et al.*, 1994). Thus a span of 28 days was specified for the model larvae to develop autonomous swimming movements making them independent of currents. We defined the survival rate as the percentage of virtual eggs that remained on the shelf (representing a chlorophyll-rich area roughly delimited by the 200-m isobath and the coast, Fig. 1) after 28 days. These rates were estimated for each of the numerical experiments considering passive Lagrangian transport (i.e., without DVM), DVM ability and the encountering of lethal temperatures for larvae during the drift period.

We repeated the release experiments using the six different years of simulation as hydrodynamic forcing and computed the average from the results. This method allowed us to evaluate the robustness of our results by estimating the impact of the unforced, intrinsic mesoscale circulation on the retention patterns.

Data

Several data products were used to evaluate the realism of the model hydrodynamics. Twelve years (October 1992 to December 2005) of sea level (or absolute dynamic topography), computed by AVISO (Archiving, Validation and Interpretation of Satellite Oceanographic data, http://www.aviso.altimetry.fr/en/data/products/sea-surface-height-products/global.html) were used to construct a monthly climatology of sea surface height (SSH) to compare with model SSH. SSH patterns, which represent streamlines of the surface geostrophic current, are used to evaluate the models' surface geostrophic circulation.

A monthly climatology (for the period January 1995 to December 2004) of 9.28 km Sea Surface Temperature (SST) from the NOAA/NASA AVHRR Oceans Pathfinder Program (version 4) (Kilpatrick *et al.*, 2001) was used. It highlights the nearshore temperature gradient typical of upwelling systems.

A monthly climatology of SeaWIFS surface chlorophyll (for the period August 1997 to February 2006) was used as a proxy to depict chlorophyll-enriched coastal regions. The climatology was constructed using data from the NASA Goddard Space Flight Center (SeaWIFS reprocessing 5, http://oceancolor.gsfc.nasa.gov/, Feldman and McClain, 2006).

RESULTS

Evaluation of hydrodynamic solutions

Sea surface temperature. The main spatial patterns as well as the seasonal cycle of SST are well captured by the two models (Fig. 2). In winter (January–March), the coolest SSTs are found along the coast (from 18°C at 22°N to 24°C near 13°N) in response to the seasonal upwelling. In summer (July–September),

Figure 2. Sea Surface Temperature (SST, °C) during winter (top) and summer (bottom) for SM1 (a, d), SM2 (b, e) model output and Pathfinder observations (c, f).

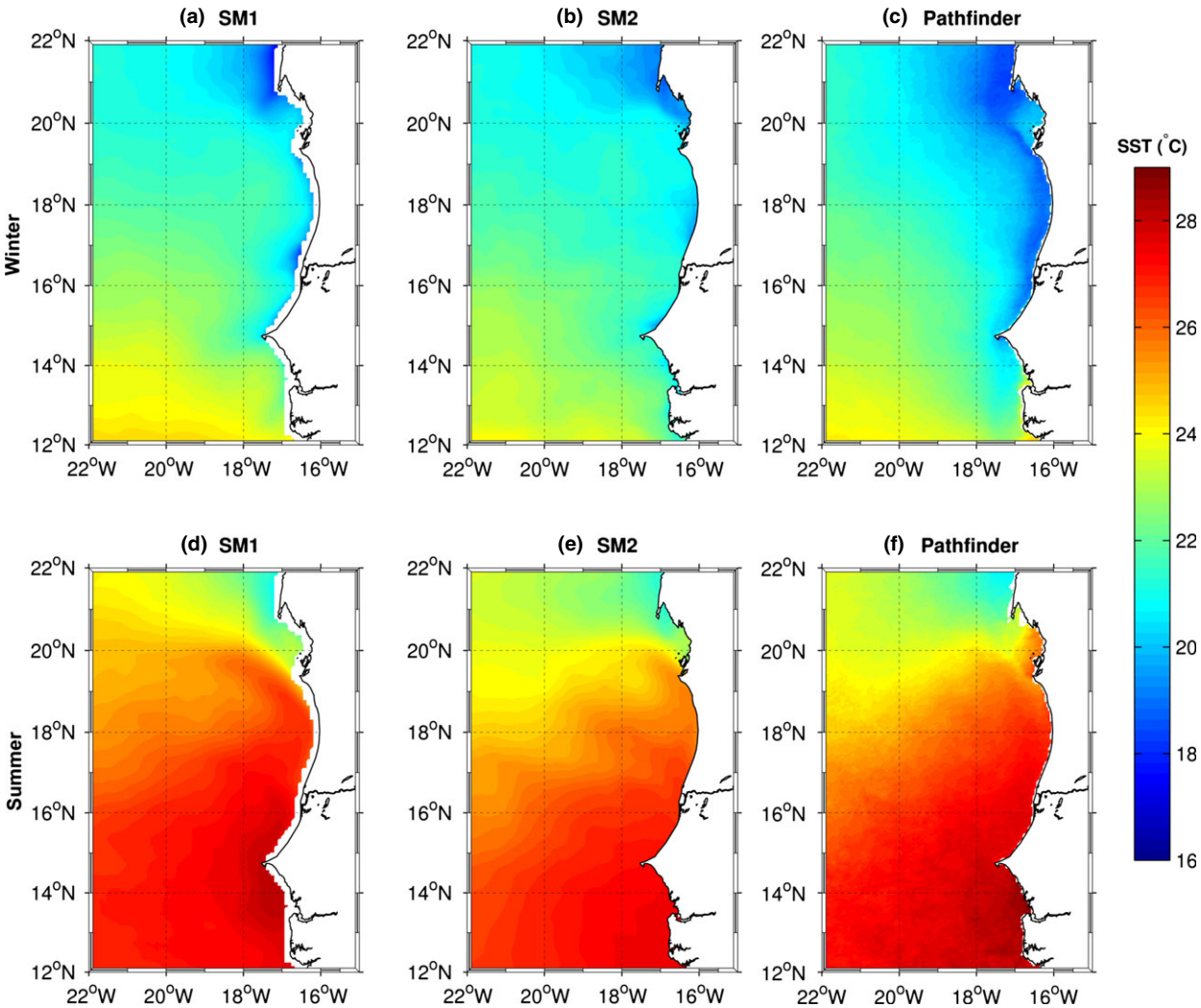

warmer SSTs along the coast (21–29°C) are encountered south of Cap-Vert owing to the northward advection of warm Guinean waters which spread over the shelf and reach Cap-Blanc (~ 21°N). Both models tend to reproduce a cold bias of ~1°C on the shelf in late fall, particularly over the central (14.75°N–19.5°N) and southern (12°N–14.75°N) regions (not shown). This bias could partly be due to an overly intense upwelling driven by uncertainties in the nearshore wind structure (Penven *et al.*, 2005; Colas *et al.*, 2011; Mason *et al.*, 2011) and/or to a warm bias in Pathfinder data evidenced in upwelling systems (Dufois *et al.*, 2012).

Sea surface height. Figure 3 shows maps of SSH from the two model runs compared with AVISO observations. In winter (January–March), the geostrophic circulation is oriented equatorward (Fig. 3a–c). The southward flow over the shelf is too intense in the central and southern regions in SM1, whereas it is more realistic in SM2. Intensification of the southward flow in SM1 may be due to a too strong upwelling caused by the narrower shelf. Indeed this may allow cold water to be upwelled closer to the coast than in SM2, thus enhancing the cross-shore density gradient which drives the equatorward geostrophic flow. In summer (July–September), the geostrophic circulation is reversed and oriented poleward (Fig. 3d–f) owing to the northward displacement of the North Equatorial Counter Current (NECC) (Mittelstaedt, 1991; Stramma *et al.*, 2005). The poleward flow forms large scale meanders near ~18–20°N in

Figure 3. Sea Surface Height Anomaly (cm) for winter (top) and summer (bottom) for SM1 (a, d), SM2 (b, e) (model output) and Aviso (satellite observations) (c, f).

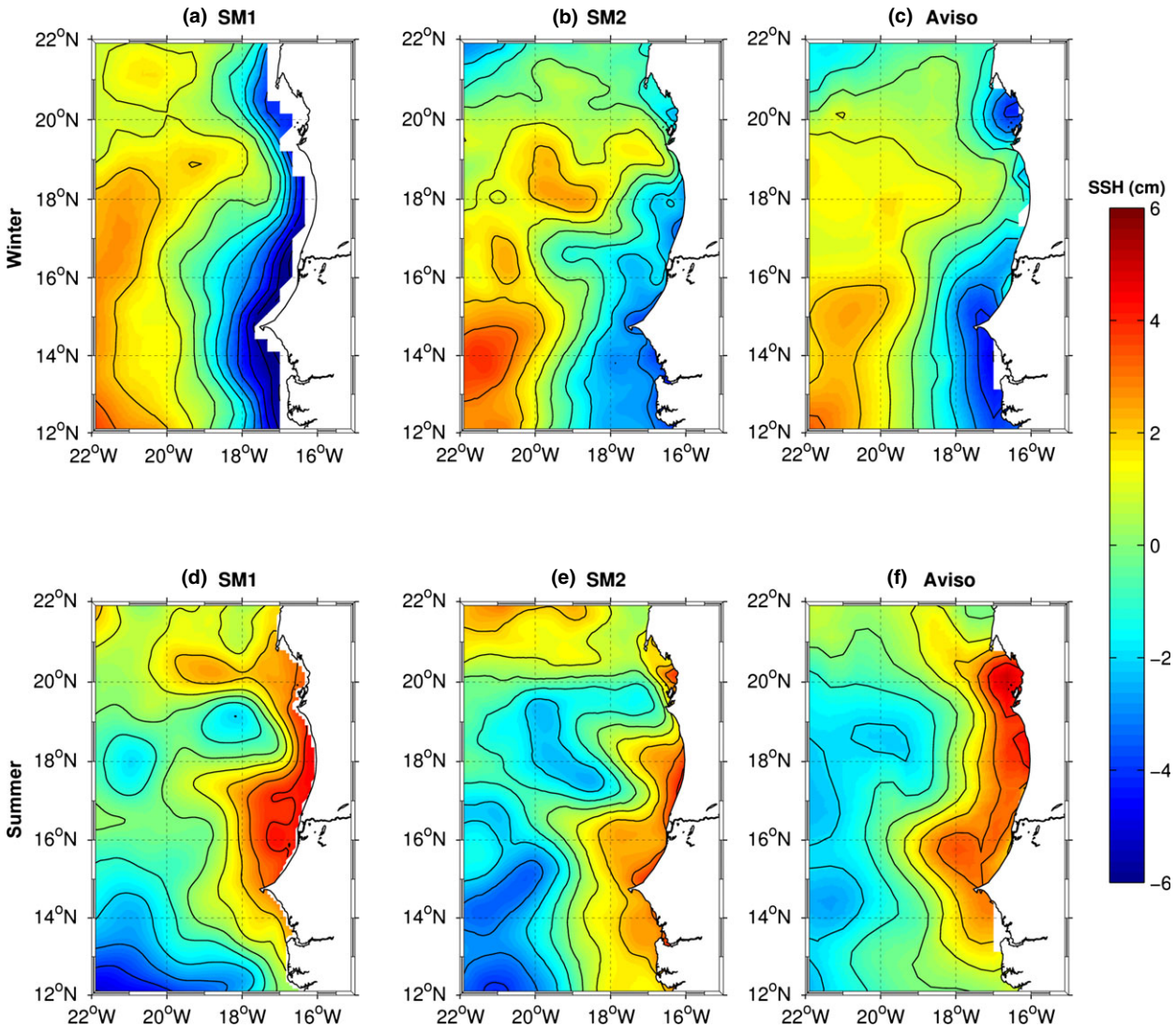

the two model runs, which are also present in the observations. This mesoscale meander creates a cyclonic eddy structure near 19°N associated with a sea level depression (Fig. 3d–f).

Larval Retention patterns. In this section we describe the mean retention patterns and emphasize the differences induced by allowing DVM. Our experiments show that lethal temperatures are rarely encountered by larvae when a critical threshold (14°C) was considered, and thus do not impact retention patterns. However, we find an impact in the case of higher lethal temperature thresholds that is discussed in the sub-section *Temporal Patterns*.

Spatial patterns. The spatial variability of the annual mean retention is shown in Fig. 4 for the passive transport (PT) Lagrangian experiment, which has similar patterns to the DVM experiments (figure not shown). Two main retention areas clearly appear. The highest retention values (60–70%) are found south of Cap-Vert (~15°N) and a second area of high retention (~30–45%) is located between 19.5°N and 21°N over the Arguin Bank. In both areas, retention is maximum nearshore. Lower retention rates (~20%) are found in the central region, which is characterized by a narrow inner shelf (Fig. 1).

Retention patterns are located in the same regions regardless of the hydrodynamic solution, but maximum

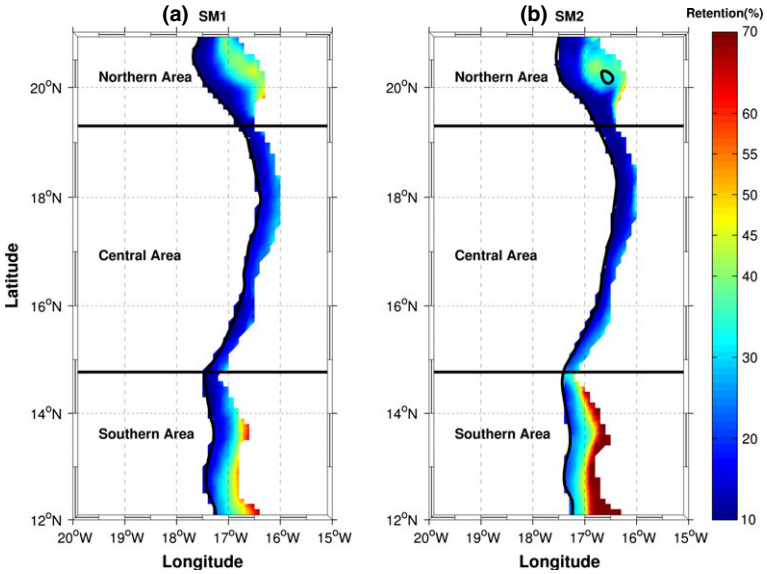

Figure 4. Annual mean shelf retention rates (% of larvae) for (a) SM1 and (b) SM2 along the Senegalese–Mauritanian coast. Results for the Passive Transport (PT) experiment are shown. Horizontal black lines mark the limit of the northern (19.5°N–21°N), central (14.75°N–19.5°N) and southern (12°N–14.75°N) retention areas (see text).

values are variable. In the southern area where retention is maximum, SM2 displays a higher retention rate than SM1 whereas the opposite occurs in the northern area.

In the northern area, rates range from 20% to 45% for SM1 and from 20% to 40% for SM2. A maximum value more than 70% is reached over a large part of the southern area for SM2 whereas it is <60% for SM1.

A cross-shore gradient of retention, which follow bathymetry, more pronounced in SM2 than in SM1, is found in the southern area. South of Casamance (~13.5°N) a retention maximum is found (90%), which extends over a larger area in SM2 than in SM1. The central area displays a similar retention rate (~20%) for both simulations.

From these spatial patterns, we define three continental shelf areas for which the seasonal variability of retention patterns is discussed: a northern area (19.5–21°N), a central area (14.75–19.5°N) and a southern area (12–14.75°N).

Temporal patterns. In this section we contrast in Fig. 5 the temporal variability of retention rates in the northern, central and southern areas as defined above. In all regions, seasonal retention rates are very similar for DVM values of 30, 60 and 100 m (Table 2), thus only results for the PT, DVM20 and DVM60 experiments are shown for clarity. The seasonality of retention rates have roughly the same patterns as for the passive transport (PT) and the different DVM values.

Maximum retention rates are found in November–December in the northern area (Fig. 5a), June–July in the central area (Fig. 5b) and from May to July in the southern area (Fig. 5c). DVM has a slightly negative effect on the number of retained particles in the northern region, whereas it has enhanced retention in the central and southern areas.

On average, by considering both DVM experiments (DVM20 and DVM60), the change in retention values is 11–16%, 23–28% and 52–66% in the northern, central and southern areas, respectively (Table 2).

Retention ranges from 10–60% for PT to 0-40% for DVM (Fig. 5a) in the northern area. In contrast, it varies from 5–40% for PT to 5–70% for DVM in the central area (Fig. 5b), and from 20–80% for PT to 30–90% for DVM in the southern area (Fig. 5c). The latter is the region of highest retention with values larger than 20% for all experiments, whereas the northern region has the lowest retention rates with almost no retention in spring and a weaker monthly variability than in regions further south (Fig. 5a). Retention increases slightly with increasing DVM depths in all regions.

Effects of lethal temperature. In this section, we study the effect of applying a lethal temperature threshold to the eggs and larvae in the three sub-regions. We tested three different lethal temperature thresholds: 14, 16 and 18°C. In Fig. 6 we present results only from DVM60 as individuals performing shallower DVM did not encounter cold waters and thus were not affected by temperature mortality. Retention rates with or without individuals experiencing lethal temperature were compared. The mortality effect increases with the lethal temperature threshold. The reasons for this

Figure 5. Seasonality of shelf retention rates (% of larvae) in three regions of the Senegalese–Mauritanian coast, for SM1 (simple lines with round marks) and SM2 (thick lines). Results for PT (red), DVM20 (green), DVM30 (blue) are shown for the northern area (a), central area (b) and southern area (c). Error bars mark the standard deviation from monthly means. Yellow rectangles indicate *a priori* observed spawning periods.

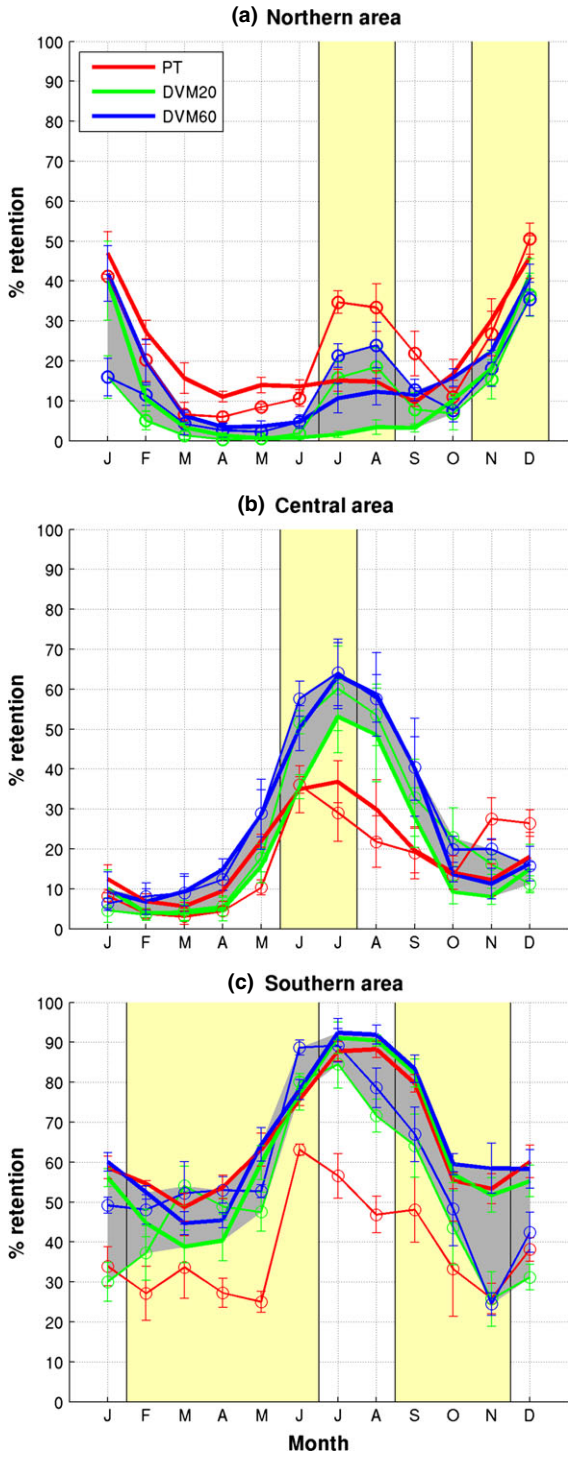

Table 2. Highlight of the mean retention from each area and for both experiments. Values from SM2 simulation is marked thicker.

	Experiment				
Area	PT	DVM20	DVM30	DVM60	DVM100
Northern area					
SMI	22.60%	10.48%	13.96%	13.35%	13.40%
SM2	**21.75%**	**11.23%**	**13.47%**	**16.09%**	**14.57%**
Central area					
SMI	16.88%	23.70%	29.30%	28.33%	27.26%
SM2	**18.48%**	**19.64%**	**23.12%**	**26.87%**	**24.76%**
Southern area					
SMI	38.23%	51.54%	56.96%	57.81%	56.80%
SM2	**64.91%**	**62.06%**	**63.77%**	**65.75%**	**65.42%**

is that in all three regions, the proportion of larvae experiencing temperatures below 14°C was low and hence did not modify the retention rates. With higher thresholds (16 and 18°C), the effect of lethal temperature is clearly seen in the different regions and also depends on the model configurations (SM1 or SM2). In the northern region, mortality was high for a lethal temperature of 18°C, and resulted in the death of almost all retained larvae from February to June (Fig. 6a, b). For other months, mortality decreased with the 16°C lethal temperature. A similar pattern of temperature mortality was found in the central region (Fig. 6c, d). The southern region displayed a large variability of temperature-dependent mortality in SM1, whereas the impact was negligible in SM2 (Fig. 6e, f). In April, all the individuals encountered temperatures lower than 18°C and subsequently died in SM1 (Fig. 6e). The retention rate dropped from ~50% without mortality to ~40% with a 16°C lethal temperature threshold. The impact was mainly evidenced during the upwelling season. Note that the 16°C intermediate temperature threshold is more likely to have a lethal effect on larval survival as the higher 18°C threshold is always reached by larvae [cold SSTs range from 18 to 24°C in winter (Fig. 2)] whereas the lowest 14°C one is rarely reached. The effect of lethal temperature mortality was enhanced in SM1 compared with SM2 owing to the narrower shelf in SM1 and hence the transport of cool waters closer to the shore (see section on *Spatial patterns*).

Larval transport and connectivity along the coast. In this subsection, we examine connectivity patterns along the coast. We evaluate the transport of eggs and larvae from their original spawning area to another favorable coastal area to the north or south. We found that the

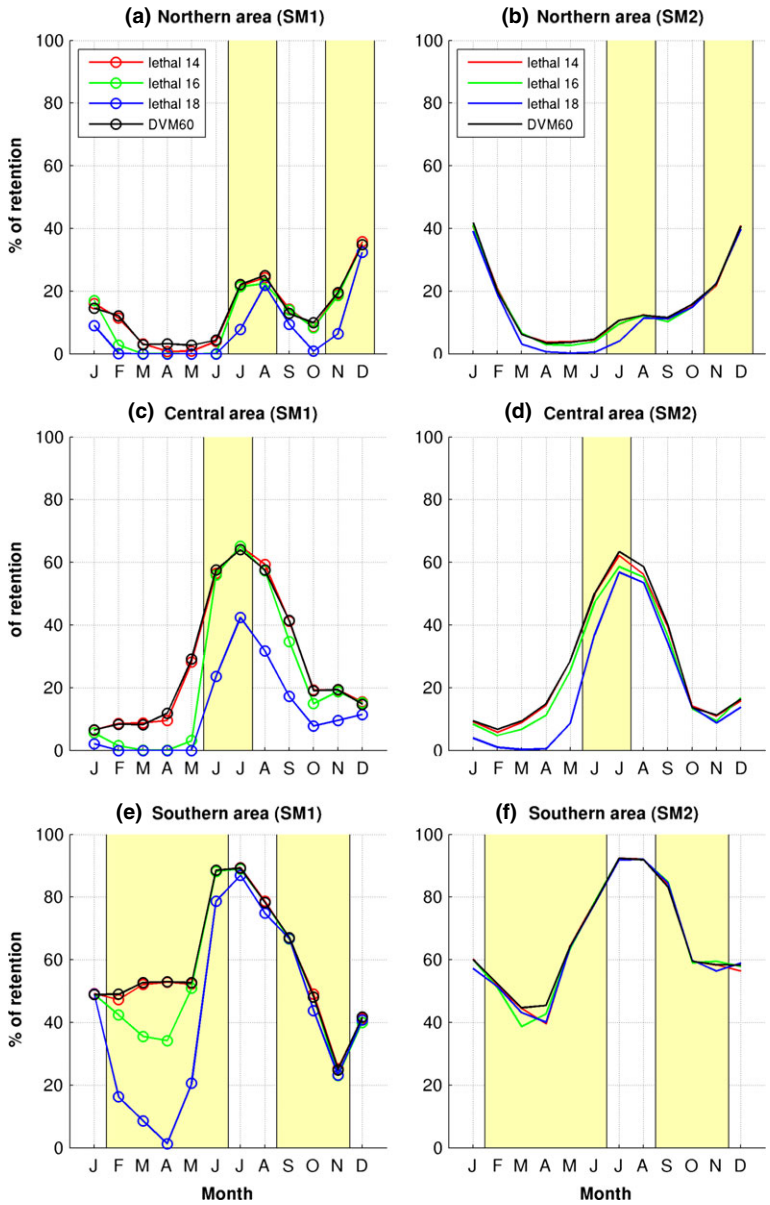

Figure 6. Seasonality of shelf retention rates (% of larvae) in the case of different lethal temperature thresholds: 14°C (red line), 16°C (green line) and 18°C (blue line). Experiments were achieved according to a DVM60 scenario for the northern (a, b), central (c, d) and southern (e, f) areas. DVM60 without any temperature effect is shown in black. SM1 and SM2 model results are shown in the left and right columns, respectively. Yellow rectangles indicate *a priori* observed spawning periods.

exchange of larvae between zones was large, mainly directed to the south, and occurred preferentially in winter–spring (Fig. 7). Our experiments show that ~50–100% of the surviving individuals (not advected offshore) released on the Arguin Bank (northern region) were transported to the shelf of the central area in late winter/spring (Fig. 7b). This proportion dropped to <30% in summer and fall. Similarly, 20–40% of surviving individuals released in the central area were transported to the southern area in winter and fall (Fig. 7d). Note that the southern drift reflects the seasonality of the upwelling, with major currents oriented southward (Rebert and Prive, 1974). Finally, eggs released in the southern area, between 55–85% (15–40%) were transported southward in winter (summer) and reached the shelf (Fig. 7f). Note that southward transport pathways from the central and southern zones were uncertain in the fall (November–December) spanning the range 0% to ~80% depending on the model (Fig. 7d–f). In contrast, northward transport of larvae from the three regions was weak and not robust as it mainly occurred in SM1 (Fig. 7a, c, e).

DISCUSSION

In this section we first discuss the potential mechanisms leading to discrepancies in retention between the two models, and then the specificities of the main

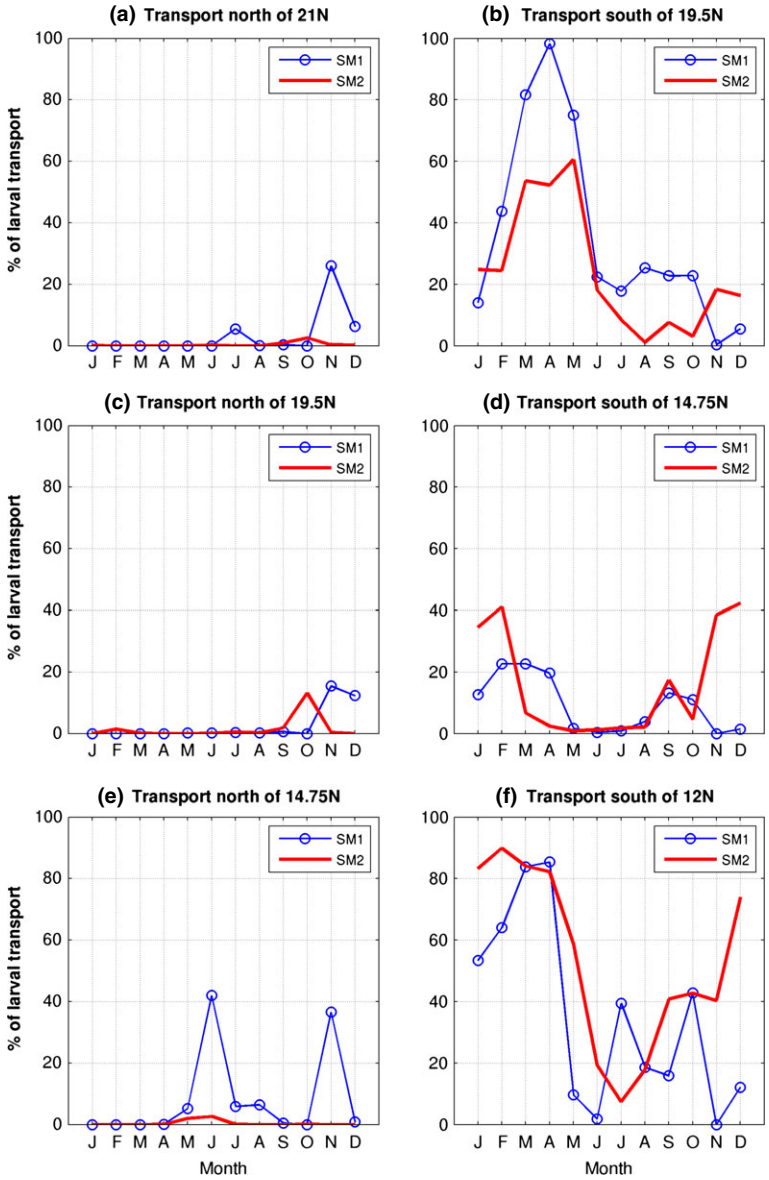

Figure 7. Exchange rate (%) for larvae reaching the northern or southern limits of their spawning areas for the northern (a, b), central (c, d) and southern (e, f) areas. SM1 and SM2 model results are shown in the left and right columns, respectively.

retention areas. The seasonality of retention in each area is compared with the observed *Sardinella aurita* spawning strategy. Satellite surface chlorophyll-a concentrations (SeaWIFS) are used as a food proxy to discuss the necessary trade-off that fish encounter when it comes to spawning in favorable retention areas or in food-enriched areas. We conclude with a discussion on the connectivity between spawning areas.

Why are there discrepancies in the retention patterns simulated by the models?

The retention patterns along the Senegalese–Mauritanian coast are quite similar in the two models although some quantitative differences are found. The northern area displays more retention for SM1, whereas retention in the southern area is enhanced for SM2 (Figs 4–5). These differences could be related to the bathymetry representation in the two models.

A large hole with depths >200 m can be seen in SM2 (Figs 4 and 10); this region is known to be shallow (Estrade, 2006). There is a notable erroneous feature at the Arguin Bank (northern region) in SM2 compared with SM1, where the bathymetry seems to be better represented, although the shallowest depth is set to 50 m. The source of this error is thought to be the version of the ETOPO2 data used for SM2. The bathymetry used for SM1 was GEBCO 1' resolution. As the retention criterion is based on particles that

remain in an area shallower than 200 m after the drift period, the particles present over the hole on the Arguin Bank in SM2 were not taken account in the retention process, which artificially reduced the retention compared with SM1. Futhermore, the dynamical effect of the hole on the circulation may also play a role. In contrast, ETOPO2 bathymetry is reliable over the rest of the domain. Bathymetry profiles in the southern area from SM1, SM2 and GEBCO observations confirm that SM2 bathymetry is more realistic than SM1 (see Figs 4, 8 and Figs S1 and S2) and a shallower shelf in SM2 may explain to some extent the higher retention in this area.

Because of differences in spatial resolution, topography smoothing and coastline definition, the surfaces located between the coast and 200-m depth used for the retention criterion differ slightly: for example the northern zone is ~18% (resp. ~7%) smaller in SM1 (resp. SM2) than in GEBCO the southern zone is ~30% (resp. 10%) smaller than GEBCO observations (Table 3). A wider shelf associated with a wider surface for retention could lead to an increased retention in the southern area in SM2.

The different wind stress products can also have an impact on retention patterns. SM1 was forced by a QuikSCAT product with a resolution of 1/2° (Liu *et al.*, 1998) whereas SM2 was forced by SCOW, a QuikSCAT product at a finer resolution (1/4°, Risien and Chelton, 2008). Wind stress is slightly more parallel to the coast in SM2 than in SM1 notably in the area off Cap-Blanc (northern area) (Fig. 9a, b), therefore more upwelling favorable. Small-scale wind stress curl patterns also differ locally at several locations (e.g., over the shelf in the southern region), potentially impacting retention. Another forcing which may explain part of the model retention discrepancies is the lateral boundary forcing. In SM2 the monthly northeast Atlantic climatology (NEAClim) of Troupin *et al.* (2010) with a resolution of 0.1° was used, where the data interpolation method allows for a better resolution of the coastal areas. Using such a fine resolution climatology may be advantageous in the southern area which is close to the southern open boundary of the SM2 model (Mason *et al.*, 2011), as opposed to lower-resolution (1°) climatologies such as WOA 2005 (Conkright *et al.*, 2002) for SM1.

Finally the SM1 currents are stronger than those of SM2, notably in deep waters (60-m depth) (Figs 10–12), the two experiments show very different cross-shore geometries, coupled with different wind forcing. These are probably the main factors inducing different cross-shore current values. The deep (minimum depth of 50 m) SM1 bathymetry and the 0.5° winds favor Ekman transport while the finer (minimum depth of 15 m) SM2 bathymetry combined with 0.25° winds (stronger curl) favor a more non-linear regime. The role of friction terms could be an additional factor, as the shallower bathymetry in SM2 would induce more friction that would impede the currents. It can be assumed that stronger currents in SM1 may increase retention capabilities with respect to SM2, and consequently compensate for its bathymetry that is less favorable for retention. This could be the reason why retention in the northern area is higher for SM1 than SM2 in summer (Fig. 5). Dedicated experiments, which are beyond the scope

Figure 8. Bathymetry profiles in the southern area (14°N) from SM1 (dark line), SM2 (blue line) and Gebco observations (red line).

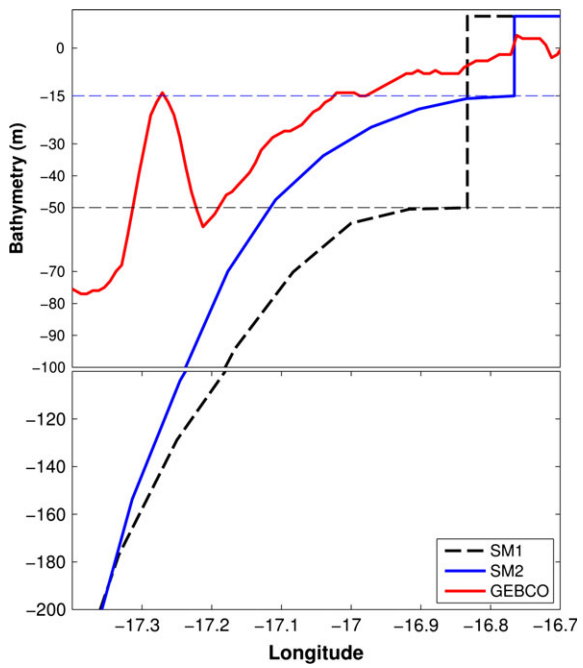

Table 3. Shelf surface reduction (%) in comparison with Gebco data for SM1 and SM2. Note that shelves (defined here by the 200 m isobath) in ROMS are always smaller than real shelves owing to horizontal smoothing of the topography.

Shelf (coast-200 m isobath) surface reduction with respect to Gebco observations	SMI	SM2
Northern area	17.5%	6.5%
Central area	29.0%	12.0%
Southern area	29.5%	10.0%

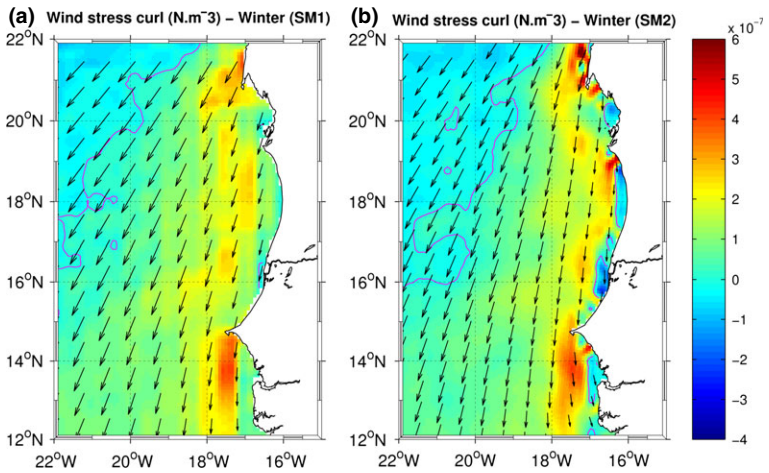

Figure 9. Wind stress (arrows, N m^{-2}) and wind stress curl (colors, N m^{-3}) from the different products (see text) forcing SM1 (a) and SM2 (b) simulations during winter (January–March). The zero wind stress curl is contoured in blue.

of the present work, would be necessary to investigate this point.

In which geographical areas does retention occur?

This study, based on tracking of model larvae, has enabled us to identify three regions of distinct retention patterns, two regions of high retention over the Arguin Bank (north of 19.5°N) and south of Cap-Vert (~14.75°N), and a region of much lower retention between these two areas (from 14.75°N to 19.5°N). These findings are consistent with previous studies. Demarcq and Faure (2000) found similar retention patterns using indices from satellite SST data. Furthermore, the two areas of highest retention appear to be closely linked to the width of the continental shelf. In the northern and southern areas, wide shelves may generate two-cell upwelling structures which enhance coastal retention. In the CCS such a structure was detected on the Saharan bank (SCOR, 1975; Salat and Cruzado, 1981; Estrade *et al.*, 2008) whereas a single upwelling cell was evidenced in the Arguin Bank (SCOR Working Group, 1975; Estrade *et al.*, 2008). This suggests that other dynamical factors may play a role in retention enhancement in this region. In contrast, Roy (1998) suggested the presence of a two-cell upwelling structure south of Senegal, potentially leading to high nearshore retention. Observations from several authors (Conand, 1977; Boely *et al.*, 1982; Fréon, 1988) also found two main spawning areas for *Sardinella aurita* located within the two highest retention areas simulated by our model.

Our Lagrangian analysis, based on circulation from two hydrodynamical models with different continental shelf widths, confirms that retention is enhanced where the shelf is larger. In our simulations, retention over the Arguin bank and, to a lesser extent, south of Cap-Vert is not clearly related to the subsurface onshore current between 20- and 50-m depth, which compensates the surface offshore Ekman current associated with the upwelling (Fig. 13). Indeed, maximum retention rates occur in the northern region during winter (Fig. 5a), whereas the onshore current is maximum in spring (March–April) in both simulations (Fig. 13a, b). In the southern region, retention is highest between June and August (Fig. 5c) during phases of weak onshore subsurface flow (Fig. 13e, f). Thus, locally increased retention appears to be more likely due to a reduction of the offshoreward current in the 0–20 m layer, clearly seen in December–January in the northern region (Fig. 13a, b) and in summer in the southern region (Fig. 13e, f) where an onshore surface current is present in the inner part of the shelf (not shown). The latter is thicker and oriented onshore for a longer time period in SM2 than in SM1 (Fig. 13e, f), which may explain maximum retention rates at the coast (Fig. 4). Low retention rates can be related to the offshore current when trade wind intensity can be very high (up to 7 m s^{-1}) (Rebert and Prive, 1974). In addition, the effects of capes along the coastline may enable nearshore retentive horizontal circulation patterns to develop (e.g., Penven *et al.*, 2000).

Note that a wide continental shelf may also have biological impacts such as limiting the action of large oceanic predators, an effect not considered here. This is especially the case in the shallow nearshore areas (Roy, 1992) where *Sardinella* larvae are present (Conand, 1977; Boely *et al.*, 1982), which are thus more favorable to juvenile survival.

How does the local circulation explain the seasonality of the retention pattern ?

Over the Arguin Bank (northern area), an offshore current flowing all year long, with maximum intensity and thickness from March to October (Fig. 13a, b),

Figure 10. Seasonal variations of the the cross-shore horizontal current (cm.s-1) averaged over the continental shelf (delimited by the 200-m isobath) in the northern (a,b), central (c,d) and southern (e,f) region for SM1 (left) and SM2 (right). Onshore (offshore) flow is represented by positive (negative) values.

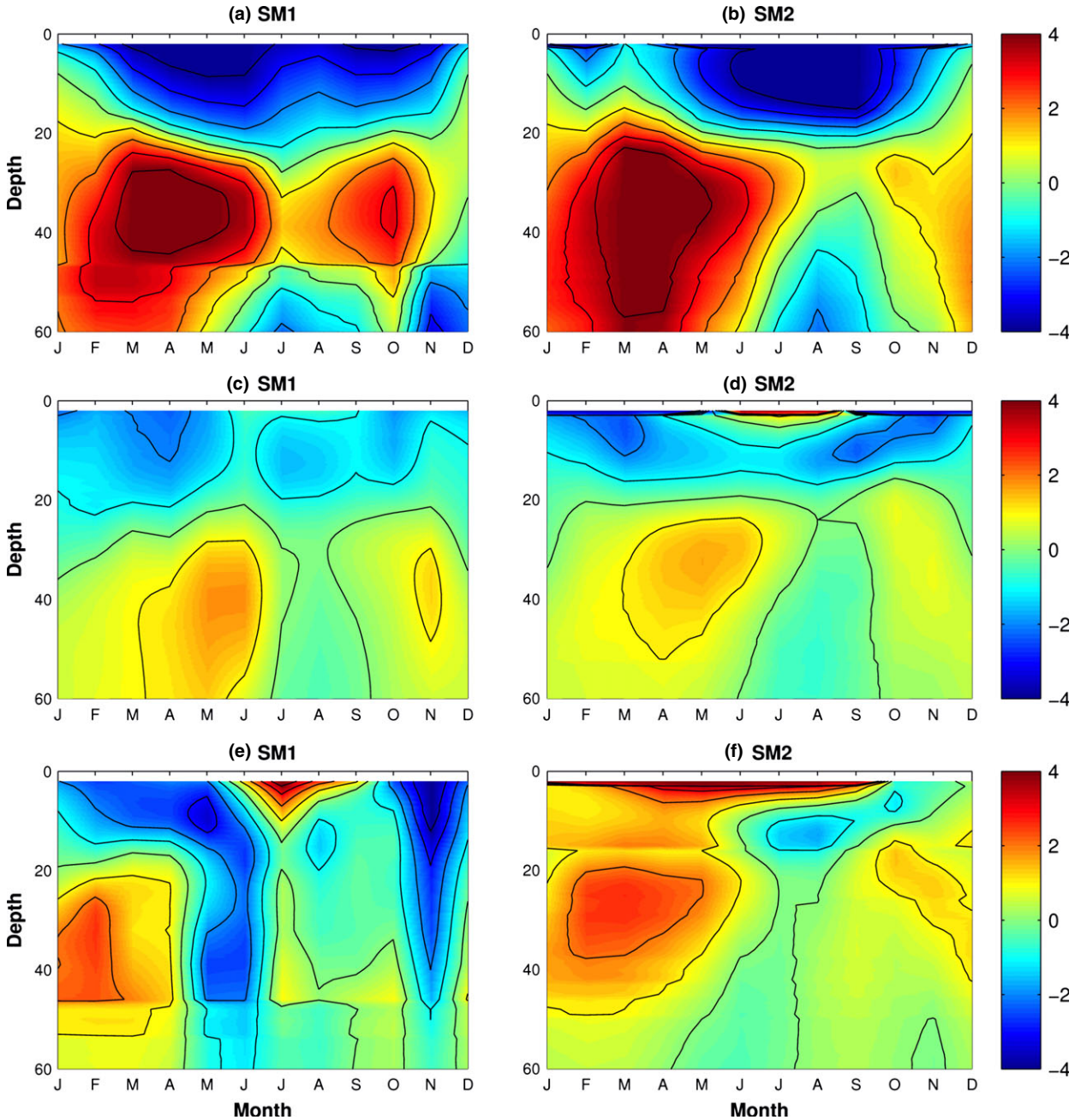

led to the lowest simulated retention rate for this area (the highest period is from November to January) (Fig. 5a). Horizontal velocity fields in May (when retention is minimum) also showed a strong offshore current in the upper and deeper layers (not shown) which transport larvae out of the domain (Fig. 13a, b). This is a consistent feature for the maximum upwelling intensity associated with this period of the year (Roy, 1992; Demarcq and Faure, 2000). This minimum retention period was related to incursions of cold upwelled waters into the area when the trade winds change their orientation and become progressively more westerly and upwelling favorable (Demarcq and Faure, 2000). The main retention period in the fall

Figure 11. Temperature (°C) and horizontal current (cm s^{-1}) at 20- (top) and 60-m (bottom) depths for SM1 (left) and SM2 (right) in December for the northern area.

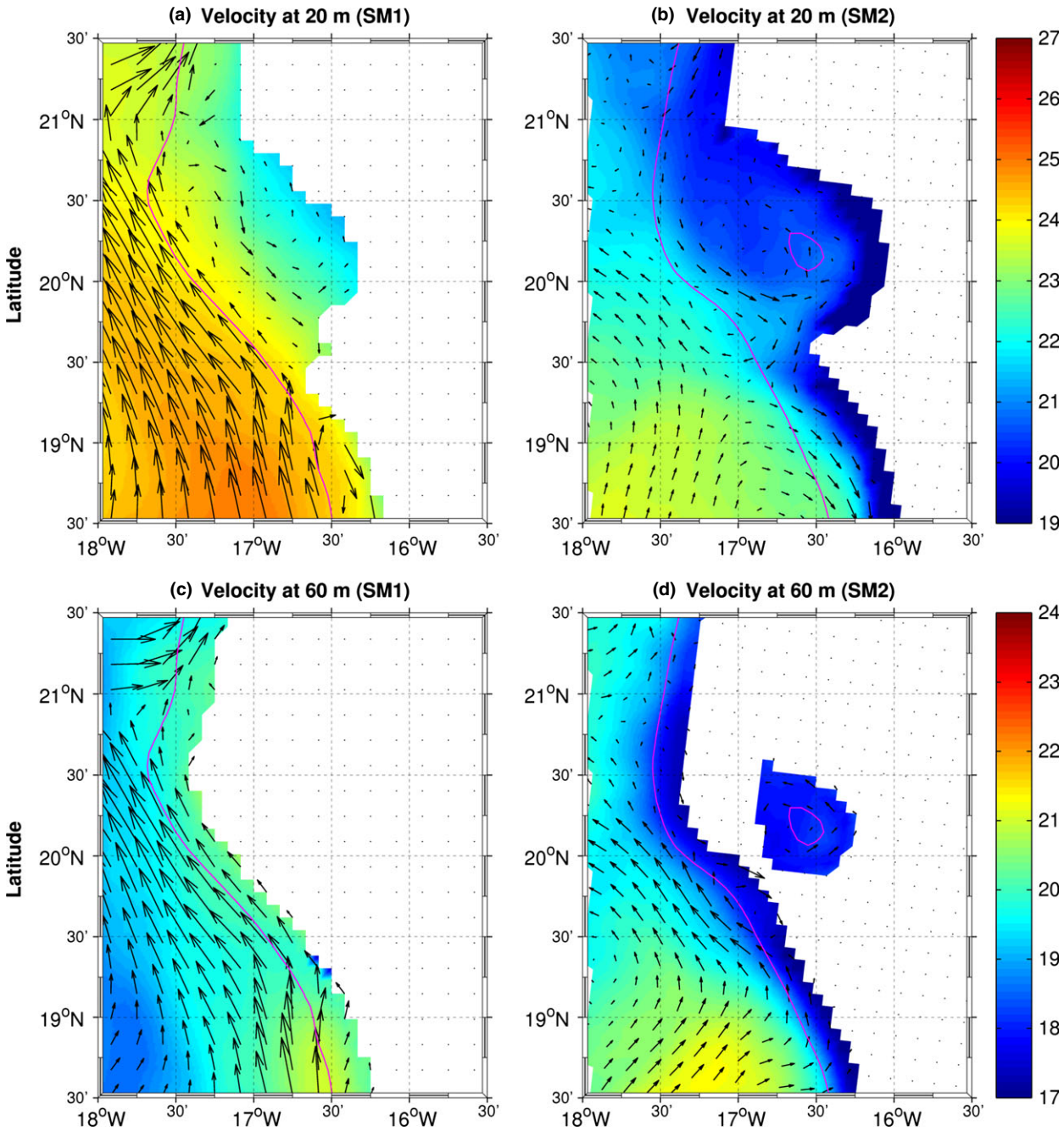

(November–December) can be explained by the presence of nearshore eddies trapping larvae over the shelf in the surface layer and by the very low surface currents (potentially due to friction) on the shallow shelf (Fig. 10a, b), combined with subsurface northward flow along the shelf edge (Fig. 10c, d).

The simulated retention peak in the central area occurred in early summer (June–July, Fig. 5b). This high retention is likely explained by the reduced offshore flow (Fig. 13c, d) and by the alongshore northward current flowing along the shelf break (Fig. 11). From October to May low retention can be related to the intensified of offshore-directed currents in the upper layer (Fig. 13c, d).

In the southern area, the main retention period in June–July results from the combined effects of an

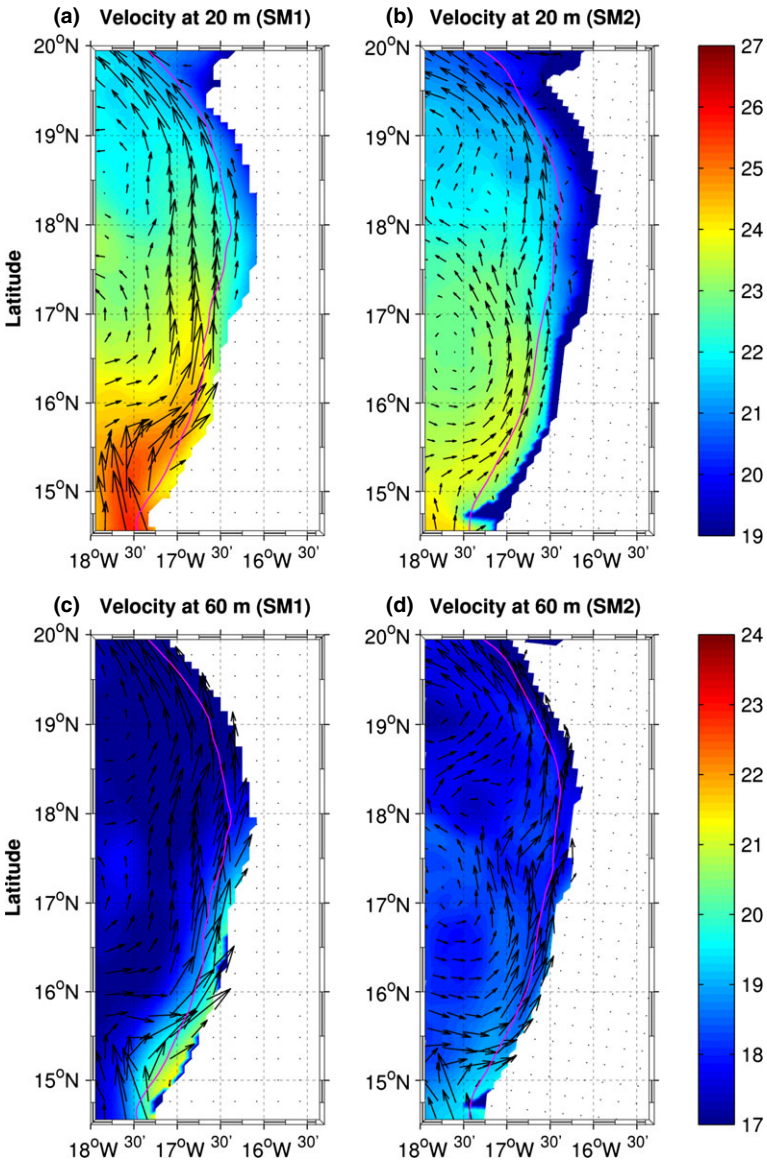

Figure 12. Same as Fig. 11, in June for the central area.

onshore current in the upper layer (Fig. 13e, f) and of the northward flow along the coast (Fig. 12a, b) and at the shelf edge (Fig. 12c, d). This northward current is probably linked to the northward displacement of the NECC, which is deflected northward by the shelf edge and forms a marked temperature front (Fig. 11a, b).

Results from Demarcq and Faure (2000) (hereafter DF) on the seasonality of retention patterns contrast with our model results notably for the northern and central area. In their study, the Arguin bank (i.e., northern area in our case) was clearly identified as a region of high retention. However, the highest retention periods occurred from March to November, whereas retention rates were maximum in December–January in our study (Fig. 5a). In the central region, DF found weak retention all year round, with slight increases in May–June and September. Consistent with our results, their retention rates were lower in the central region than in the northern and southern regions. Note that the central region in DF corresponds to the southern part of our central area, which may explain some of the discrepancies. In the southern area, retention in DF is consistent with our results. It displays higher retention indices than in the central region all year round and reaches maximum values from January to June. Some of the differences can be related to the use of retention indices based on satellite SST data that omit the vertically sheared currents which play a crucial role in our simulations. Furthermore, by nature, this thermal retention index is not

Figure 13. Same as Fig. 11, in June for the southern area.

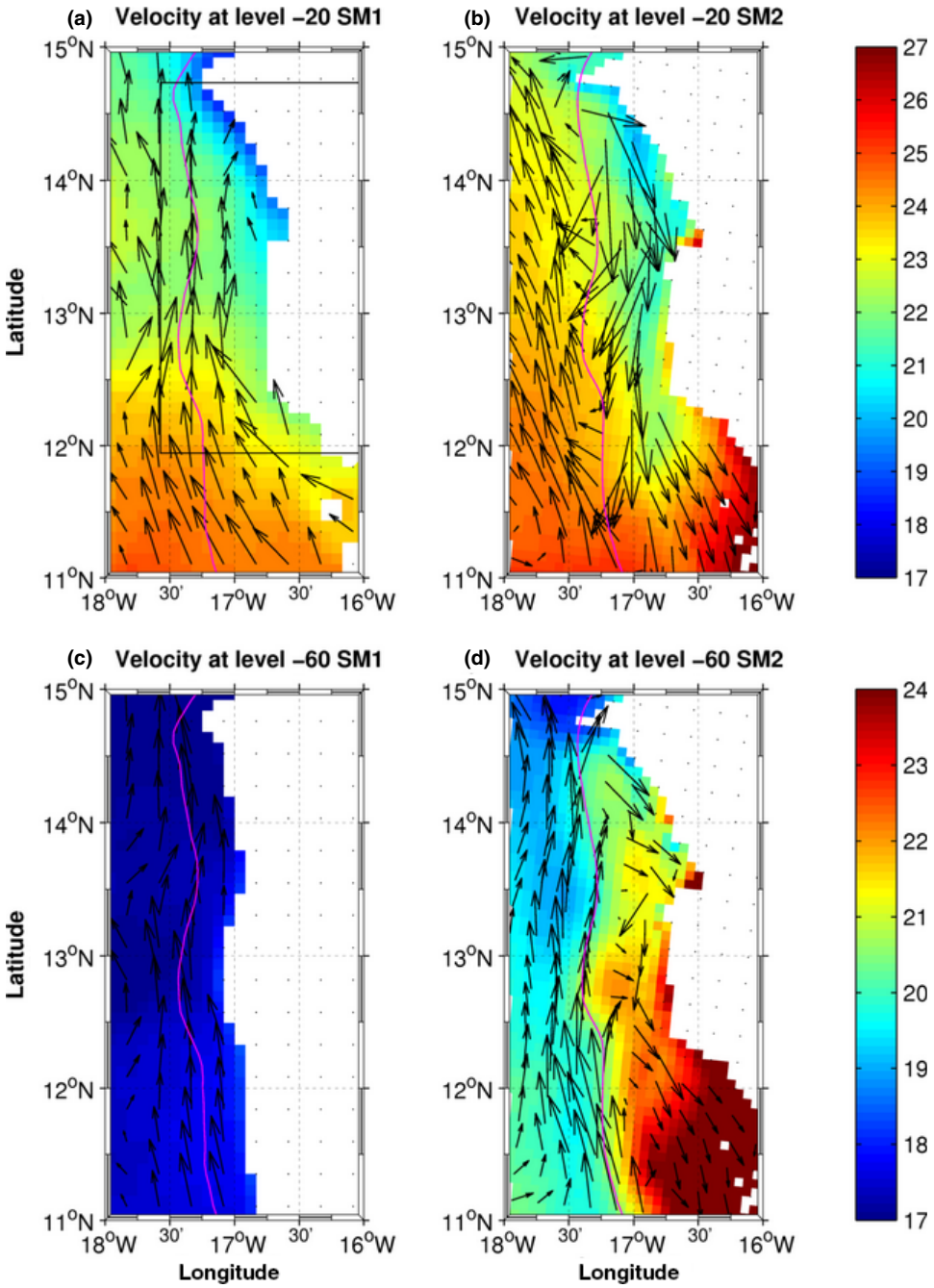

defined when the coastal upwelling does not occur, especially from July to August for most areas.

Do retention patterns coincide with known spawning patterns?

The seasonality of retention broadly matches the spawning period of *Sardinella aurita* in the northern area (Fig. 5a). Spawning has been observed in July–August and November–December (Boely *et al.*, 1982; Taleb, 2005) in this area. These periods coincide with the two favorable retention periods simulated in the present study. The seasonal variability of mean chlorophyll-a concentration over the Arguin Bank is low with values always >4 mg Chl m^{-3}, (Fig. 14a) and higher from June to November (>6 mg Chl m^{-3}), in agreement with Taleb (2005), whereas retention peaks

Figure 14. SeaWIFs surface chlorophyll (mg Chl m^{-3}, green line) averaged between the coast and the 200-m isobath, retention of living (thick blue line with round marks) and dead (thin blue line) larvae for the northern (a), central (b) and southern (c) areas. Experiment using DVM60 and a lethal temperature of 16°C are shown. Yellow rectangles indicate *a priori* observed spawning periods.

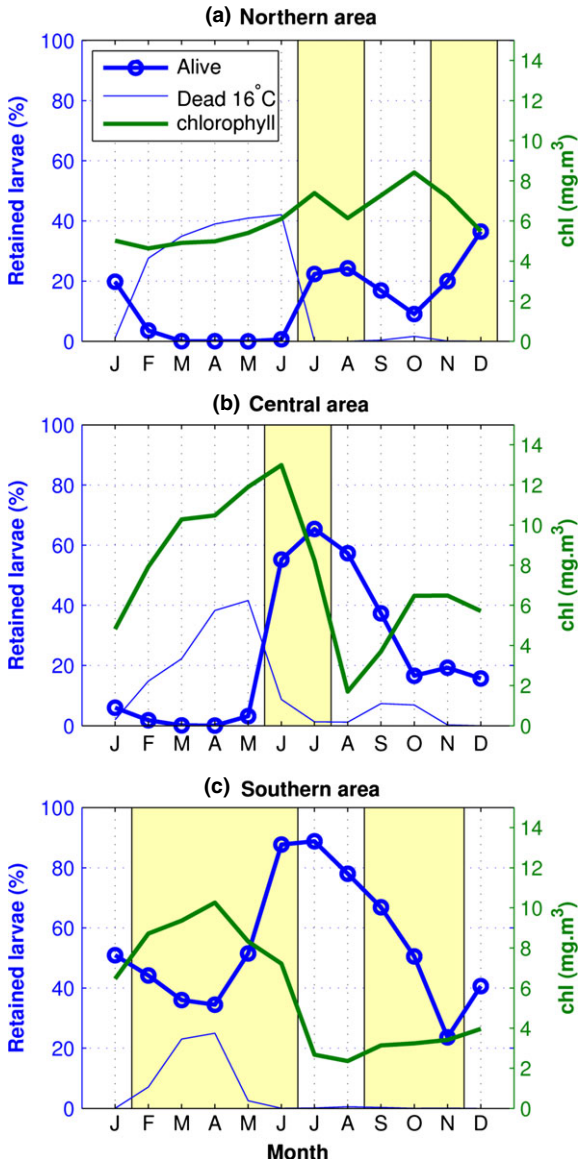

in July–August and November–December (Fig. 5a). We conclude that over the Arguin Bank, the *Sardinella aurita* reproduction strategy is probably optimized to avoid cooler temperatures and to optimize retention (Fig. 14a). As primary production is constantly high over the Arguin Bank, it is unlikely to be a limiting factor in larvae survival.

In the central area spawning was observed during summer (June–July; Boely *et al.*, 1982) which corresponds to the simulated retention peak (Fig. 5b). Taking food availability into account, chlorophyll peaked during the same period (Fig. 14b), thus spawning in the central area matches high retention and chlorophyll peaks in summer. Note that chlorophyll concentration remained high throughout the year particularly during winter–spring, when retention rates were low. This suggests that retention, rather than forage availability, is the limiting factor in the central area.

In the southern area the main observed spawning period occurs during the upwelling season, from February to June, with a peak in May–June and a secondary peak before the upwelling season in September–November (Boely *et al.*, 1982; Fréon, 1988). Recently, Ndiaye (2013), analyzing the fluctuations of gonadosomatic indices of *Sardinella aurita* adults south of Senegal using data collected between March 2012 and February 2013, confirmed that spawning did not occur in July–August but rather in February–June and November–December. The February–June period corresponds to the period of increasing retention but not to its maximum, which occurs in July–August (Fig. 5c). The second spawning period observed in September–December (Boely *et al.*, 1982; Ndiaye, 2013) coincided with high retention, especially in the SM2 model (~60%), whereas retention strongly decreased in SM1 (from ~60% in September to ~20% in November, Fig. 5c). Hence there remains large uncertainties in our evaluation of retention during this season. The period of maximum retention in our simulations corresponds to the period of minimum surface chlorophyll-*a* concentrations (Fig. 14c), which might explain why spawning is not observed in July–August. As this region is relatively favorable to retention during the entire year (>40%; Fig. 5c), retention might not be the limiting factor for reproduction success. Spawning strategies may favor the period of highest food availability with risk of larvae mortality owing to the effect of lethal temperature (Fig. 14c), disregarding the period of highest retention during which unfavorable hydrological (warm temperature) and biological (low chlorophyll *a* concentrations) conditions are encountered. Indeed, *Sardinella aurita* optimal spawning conditions were found with temperatures ranging from 22 to 25°C between April and June (Conand, 1977). These conditions were encountered in the southern area (not shown) and coincide with maximum chlorophyll concentrations in spring (Fig. 14c).

Sardinella aurita spawning peaks were observed in spring in the southern area, in June–July in the central area and then in July–August in the northern area

(Fig. 5), which is consistent with the observed northward migration of spawning adults (Boely *et al.*, 1982). This migration, allowing adults to reach optimal spawning conditions from south to north is consistent with our model results, which show high retention rates (with high absolute values) in the south throughout most of the year, in May–October in the central region, and in July–August and December–January in the northern region. Note that the absolute values of retention favor the southern area which may explain the much longer favorable period. Furthermore, the shorter spawning periods in September–November in the southern area and in June–July in the central area are probably due to limitation by food availability during the shutdown of upwelling in summer.

To which coastal areas are larvae preferentially transported?

In this section, we discuss the connectivity between sub-regions and between known spawning areas located north and south of our region of interest. A spawning area has been reported north of the Arguin Bank, over the Saharan Bank (~21–23°N) for *Sardinella aurita* and *S. Maderensis* (Ettahiri *et al.*, 2003). Based on our model results, exchange of larvae from the Arguin Bank to the Saharan Bank was weak (except for 20% in November for SM1, Fig. 7a), which suggests a weak larval connectivity between these two regions. However larval transport from this spawning area to the Arguin Bank was not quantified in this study. As larval transport would be mainly southward owing to the presence of the Canary Current over the Saharan Bank (Arístegui *et al.*, 2009), larval connectivity between these two areas may take place during the upwelling season.

In contrast, during the upwelling season (winter–spring), 50% to 100% of ichthyoplankton released over the Arguin Bank and retained over the shelf were transported to the central area (Fig. 7b) by the southward coastal current. During the same time period chlorophyll concentrations were highest over the whole domain (~8–12 mg Chl m^3; Fig. 14b). This combination of larval transport from the northern area and the presence of food make the central area a good candidate as a nursery area during the cold season (February–May). Indeed Conand and Fagetti (1971) showed that large sardinella larvae (> 14 mm) were found north of Cap-Vert during this period, suggesting that larvae from the northern area could have accumulated in the central area. However, only a small number of such larvae were observed in this region (Conand and Fagetti, 1971). As suggested by our sensitivity test, this might be due to the larval lethal temperature limitation (see section *Effects of lethal temperature*, Fig. 14b).

Nursery areas of *Sardinella aurita* off Guinea (~10°N) have not been identified but, as the shelf remains wide, retentive processes could occur and favor the survival of the transported larvae.

Marchal (1991) reported the presence of *Sardinella aurita* larvae as far south as Cap-Palmas (~5°N) in March, where the so-called Ivory Coast upwelling is active (Colin, 1988; Binet and Servain, 1993). The length of the collected larvae was notably greater than that of those collected further east near Cap Three Points off Ghana. Therefore, considering that larvae may survive during their southward transit, larval connectivity from the southern area to the spawning region off Cap-Palmas (~5°N) (Marchal, 1993) could occur. Unfortunately the hypothesis of connectivity with the Ivory Coast upwelling region could not be verified as our southern model domain limit is at 8°°N. This is a perspective for future work.

CONCLUSIONS

The aim of this study was to investigate the influence of environmental conditions on *Sardinella aurita* larval transport off the Senegalese–Mauritanian coast and to compare their spawning patterns with modeled retention patterns.

The *Sardinella aurita* spawning season in the northern (19.5°N–21°N) and central (14.75°N–19.5°N) areas matches the period of high retention and high surface chlorophyll. The southern area (12°N–14.75°N) has the highest retention rates. In this subregion, spawning matches the period of maximum chlorophyll but not the season of maximum retention (summer). During the maximum retention period, the upwelling relaxes in this area and phytoplanktonic biomass reaches its lowest values. We suggest that retention, associated with food availability, plays an important role in *Sardinella aurita* spawning, and potentially for any pelagic species with planktonic stages within a similar habitat. This is particularly clear in the central area, where retention and chlorophyll peaks coincide whereas cooling, leading to lethal temperature exposure, is the limiting factor during the upwelling season. The intermediate 16°C temperature is suggested to underline the effect of lethal temperature on larvae and thus impact on spawning patterns. This value is mainly a parametric test and needs to be validated by observations.

A significant proportion of larvae are transported from the northern shelf to the central area in winter–spring, combined with substantial availability of food

(high chlorophyll), suggesting that this region may be a nursery area for *Sardinella aurita* during the cold season (although low temperatures may be a limiting factor). Such areas can help in the definition of protected areas for larvae and juveniles development, i.e., Marine Protected Areas (MPA). Connectivity through larval transport may exist between the southern Senegal spawning area and the Cap-Palmas nursery area off Liberia. The modeled exchanges are valid for any species with planktonic stages. The important connectivity revealed in this study underlines the need for call to a joint management of shared stocks, particularly the small-pelagic fisheries which are crucial to the economy of neighboring West African countries.

The relatively low retention rates found over the Arguin Bank, together with possible thermal limitation for larval development, suggest limited yearly reproductive success and, hence, a limited contribution from this area to the total *Sardinella aurita* recruitment off west Africa. In contrast, the southern area displays higher retention rates and virtually no low temperature limitations. This suggests a major contribution of this spawning area to total recruitment.

Our results are somewhat limited by the resolution of the hydrodynamical models (~7.5–8 km), which do not realistically reproduce the sub-mesoscale ocean dynamics over the shelf. In future work we will study retention with increased model resolution (~1–3 km) in the Senegalese–Mauritanian area as sub-mesoscale features may play an important role on productivity and on larval transport. Furthermore, the introduction of a bioenergetic model for larval growth will allow us to further investigate biological effects on reproductive success [e.g., by representing different vertical migration regimes as functions of larvae size (Ospina-Alvarez *et al.*, 2012)].

ACKNOWLEDGMENTS

This work is a contribution to the complex modeling systems program PDI-MSC/UMMISCO. This investigation was supported by funding from the Institut de Recherche pour le Developpement (IRD) and Université Pierre et Marie Curie (UPMC). The authors are grateful to the Laboratoire Mixte International 'Etude du Climat de l'Afrique de l'Ouest' (LMI-ECLAIR) and to Université de Bretagne Occidental (UBO) for facilitating travel from Dakar to Paris and Brest, which permitted stronger interactions between the principal investigators of this study, and allowed us to use more powerful computing facilities than locally available. The SM2 solution was developed at UCLA, where ROMS development is supported by the Office of Naval Research (currently grant N00014-08-1-0597); this work was partially supported by the National Center for Supercomputing Applications under grant number OCE030007 and utilized the *abe* system. Evan Mason is supported by a Spanish government JAE-Doc grant (CSIC), cofinanced by FSE. We are grateful to the anonymous reviewer for his helpful comments. The authors want to acknowledge Modou Thiaw (CRODT, Dakar) and Vamara Koné (CRO, Abidjan) for fruitful discussions.

REFERENCES

Arístegui, J., Alvarez-Salgado, X.A., Barton, E.D. *et al.* (2006) Oceanography and fisheries of the Canary Current Iberian region of the Eastern North Atlantic. In: The Global Coastal Ocean: Interdisciplinary Regional Studies and Syntheses, The Sea:Ideas and Observations on Progress in the Study of the Seas, vol. 14. A., Robinson & K.H. Brink (eds) Harvard University Press, pp. 877–931.

Arístegui, J., Barton, E.D., Álvarez-Salgado, X.A. *et al.* (2009) Sub-regional ecosystem variability in the canary current upwelling. *Prog. Oceanogr.* **83:**33–48.

Bakun, A. (1996) Patterns in the Ocean: Ocean Processes and Marine Population Dynamics. San Diego, California, USA: University of California Sea Grant, in cooperation with Centro de Investigaciones Biologicas de Noroeste, La Paz, Baja California Sur, Mexico. 323 pp.

Barnier, B., Siefridt, L. and Marchesiello, P. (1995) Thermal forcing for a global ocean circulation model using a three-year climatology of ECMWF analyses. *J. Mar. Syst.* **6:**363–380.

Binet, J. and Servain, J. (1993) Have the recent hydrological changes in the northern Gulf of Guinea induced the *Sardinella aurita* outburst? *Oceanol. Acta* **16:**247–258.

Boely, T. (1979) Biologie des deux espèces de sardinelles (*Sardinella aurita* Val. 1847 et Sardinella maderensis Lowe 1841) des côtes sénégalaises. Thèse de doctorat. Université de Paris VI et M.N.H.N. Paris.

Boely, T., Chabanne, J., Fréon, P. *et al.* (1978) Cycle sexuel et migration de Sardinella aurita sur le plateau ouest-africain des îles Bissagos à la Mauritanie. Symposium sur le courant des Canaries, upwelling et ressources vivantes, Las Palmas 11–14 avril 1978 **92:** 12.

Boely, T., Chabanne, J., Fréon, P. *et al.* (1982) Cycle Sexuel et Migrations de *Sardinella aurita* sur le Plateau Continental Ouest-africain, des Iles Bissagos à la Mauritanie. Rapport. P.V. Réunion du Conseil International pour l'Exploration de la Mer **180:**350–355.

Brochier, T., Lett, C., Tam, J. *et al.* (2008a) An individual-based model study of anchovy early life history in the northern humboldt current system. *Prog. Oceanogr.* **79:**313–325.

Brochier., T., Azeddine Ramzi, A., Christophe Lett, C. *et al.* (2008b) Modelling sardine and anchovy ichthyoplankton transport in the canary current system. *J. Plankton Res.* **30:**1133–1146.

Colas, F., McWilliams, J.C., Capet, X. *et al.* (2011) Heat balance and eddies in the peru-chile current system. *Clim. Dyn.* **39:**509–529.

Colin, C. (1988) Coastal upwelling events in front of the Ivory Coast during the FOCAL program. *Oceanol. Acta* **11:**125–138.

Conand, F. (1977) Oeufs et Larves de la Sardinelle Ronde (*Sardinella aurita*) au Sénégal: Distribution, Croissance Mortalité, Variations D'abondance de 1971 à 1976. *Cah. ORSTOM Sér. Océanogr.* **15:**201–214.

Conand, F. and Fagetti, E. (1971) Description et distribution saisonnière des larves de sardinelles des côtes du Sénégal et de la Gambie En 1968 et 1969. *Cah. ORSTOM Sér. Océanogr.* **9:**293–318.

Conkright, M.E., Locarnini, R.A., Garcia, H.E. *et al.* (2002) World Ocean Atlas 2001: Objectives, Analyses, Data Statistics and Figures [CD-ROM]. Silver Spring, MD: NOAA Atlas NESDIS 42.

Corten, A., Mendy, A.N. and Diop, H. (2012) The sardinella of northwest Africa: fisheries, stock assessment and management. Doc. tech. Sub-regional Fisheries commission.

Cury, P. and Roy, C. (1989) Optimal environmental window and pelagic fish recruitment success in upwelling areas. *Can. J. Fish Aquat. Sci.* **46:**670–680.

Cury, P., Bakun, A., Crawford, R.J.M. *et al.* (2000) Small pelagics in upwelling systems: patterns of interaction and structural changes in 'wasp-waist' ecosystems. *ICES J. Mar. Sci.* **57:**603–618.

Cury, P., Shin, Y.J., Planque, B. *et al.* (2008) Ecosystem oceanography for global change in fisheries. *Trends Ecol. Evol.* **23:**338–346.

Da Silva, A.M., Young, C.C. and Levitus, S. (1994) Atlas of surface marine data 1994. Vol. 3, Anomalies of heat and momentum fluxes; Vol. 4, Anomalies of freshwater fluxes, NOAA Atlas, NESDIS 4, 413 pp.

De Boyer Montégut, C., Madec, G., Fischer, A.S. *et al.* (2004) Mixed layer depth over the global ocean: an examination of profile data and a profile-based climatology. *J. Geophys. Res.* **109:**C12003.

Debreu, L., Marchesiello, P., Penven, P. and Cambon, G. (2012) Two-way nesting in split-explicit ocean models: algorithms, Implementation and Validation.. *Ocean Model.* **49–50:**1–21.

Demarcq, H. (1998) Spatial and temporal dynamic of the upwelling off Senegal and Mauritania: local change and trend. In: Global Versus Local Changes in Upwelling Systems. M.H. Durand, P. Cury, R. Mendelssohn, C. Roy, A. Bakun & D. Pauly (eds) Paris: ORSTOM, pp. 149–166.

Demarcq, H. and Faure, V. (2000) Coastal upwelling and associated retention indices derived from satellite SST. Application to *octopus vulgaris* recruitment. *Oceanol. Acta* **23:**391–408.

Dias, D.F., Pezzi, L.P., Gherardi, D.F.M. *et al.* (2014) Modeling the spawning strategies and larval survival of the Brazilian sardine (*Sardinella Brasiliensis*). *Prog. Oceanogr.* **123:**38–53.

Ditty, J.G., Houde, E.D. and Shaw, R.F. (1994) Egg and larval development of spanish sardine, *Sardinella Aurita* (Family Clupeidae), with a synopsis of characters to identify clupeid larvae from the Northern Gulf of Mexico. *Bull. Mar. Sci.* **54:**367–380.

Dufois, F., Penven, P., Whittle, C.P. *et al.* (2012) On the warm nearshore bias in pathfinder monthly sst products over eastern boundary upwelling systems. *Ocean Model.* **47:**113–118.

Estrade, P. (2006) Mécanisme de Décollement de L'upwelling Sur Les Plateaux Continentaux Larges et Peu Profonds d'Afrique Du Nord-Ouest. Brest, France: Thèse de doctorat Université de Bretagne Ocidentale.

Estrade, P., Marchesiello, P., Colin De Verdière, A. *et al.* (2008) Cross-shelf structure of coastal upwelling: a two dimensional extension of ekman's theory and a mechanism for inner shelf upwelling shut down. *J. Mar. Res.* **66:**589–616.

Ettahiri, O., Berraho, A., Vidy, G., *et al.* (2003) Observations on the spawning of Sardina and Sardinella off the south Moroccan Atlantic coast (21–26°N). *Fish. Res.* **60:** 207–222.

FAO. (2012) Report of the working Group on the assessment of small-pelagic fish off northwest Africa. FAO Fisheries Report 1036:3pp.

Feldman, G.C and McClain, C.R. (2006) SeaWIFS reprocessing 5, URL http://oceancolor.gsfc.nasa.gov/. [accessed 3 December 2013].

Fréon, P. (1988) Réponses et adaptations des stocks de Clupéidés d'Afrique de l'Ouest à la variabilité du milieu et de l'exploitation. Etudes et Thèses. ORSTOM Editions, 287 p.

Fréon, P., Alheit, J., Barton, E.D. *et al.* (2006) Modelling, forecasting and scenarios in comparable upwelling ecosystems: California, Canary and Humboldt. In: G. Hempel, C. Moloney, P. Rizzoli, J. Woods (Eds.). The Benguela. Predicting a Large Marine Ecosystem. Elsevier Series, Large Marine Ecosystems, Vol **14:**185–220.

Kilpatrick, K.A., Podestá, G.P. and Evans, R. (2001) Overview of the NOAA/NASA advanced very high resolution radiometer pathfinder algorithm for sea surface temperature and associated matchup database. *J. Geophys. Res.* **106:** 9179–9197.

Lasker, R. (1975) Field criteria for survival of anchovy larvae-relation between inshore chlorophyll maximum layers and successful 1st feeding. *Fish. Bull.* **73:**453–462.

Lasker, R. (1978) The relation between oceanographic conditions and larval anchovy food in the California Current: identification of factors contributing to recruitment failure. *Rapport du procès verbal de la Réunion du conseil international pour l'exploration de la mer.* **173:**212–230.

Lathuilière, C., Vincent, E. and Marina, L. (2008) Seasonal and intraseasonal surface chlorophyll-a variability along the Northwest African Coast. *J. Geophys. Res.* **113:**C05007.

Lett, C., Roy, C., Levasseur, A. *et al.* (2006) Simulation and quantification of enrichment and retention processes in the southern benguela upwelling ecosystem. *Fish Oceanogr.* **15:**363–372.

Lett, C., Verley, P., Mullon, C. *et al.* (2008) A Lagrangian tool for modelling ichthyoplankton dynamics. *Environ. Model. Softw.* **23:**1210–1214.

Liu, W.T., Tang, W. and Polito, P.S. (1998) Nasa scatterometer provides global ocean-surface wind fields with more structures than numerical weather prediction. *Geophys. Res. Lett.* **25:**761–764.

Machu, E., Ettahiri, O., Kifani, S., *et al.* (2009) Environmental control of the recruitment of sardines (*Sardina Pilchardus*) over the Western Saharan shelf between 1995 and 2002: a coupled physical/biogeochemical modelling experiment. *Fish Oceanogr.* **18:**287–300.

Marchal, E. (1991) Un Essai de Caractérisation Des Populations de Poissons Pélagiques Côtiers: Cas de Sardinella Aurita Des Côtes Ouest Africaines. In: Pêcheries ouest-africaines.

Variabilité, instabilité et changement. P. Cury et C. Roy (eds) Paris: ORSTOM, pp. 192–200.
Marchal, E. (1993) Biologie et Écologie des poissons pélagiques côtiers du littoral Ivoirien. In: Environnement et ressources aquatiques de Côte d'Ivoire: 1. Le milieu marin. P. Le Loeuff, E. Marchal & J.B. Amon Kothias (eds) Paris: ORSTOM, pp. 237–270.
Mason, E., Molemaker, J., Shcheptekin, A. *et al.* (2010) Procedures for offline grid nesting in regional ocean models. *Ocean Model.* **35:**1–15.
Mason, E., Colas, F., Molemaker, J. *et al.* (2011) Seasonal variability of the canary current: a numerical Study. *J. Geophys. Res.* **116:**C06001.
Marta-Almeida, M., Dubert, J., Peliz, A., *et al.* (2006) Influence of vertical migration pattern on retention of crab larvae in a seasonal upwelling system. *Mar. Ecol. Prog. Ser.* **307:**1–19.
Matsuura, Y. (1971) A Study of the Life History of Brazilian Sardines, Sardinella Aurita. I. Distribution and Abundance of Sardine Eggs in the Region of Ilha Grande, Rio de Janeiro. *Bolm. Inst. Oceanogr. S. Paulo* **20:**33–60.
Matsuura, Y. (1975) A study of the life history of brazilian sardine, sardinella brasiliensis: III. Development of sardine larvae. *Boletim Do Instituto Oceanográfico* **24:**17–29.
Mittelstaedt, E. (1991) The ocean boundary along the northwest African Coast: circulation and oceanographic properties at the sea surface. *Prog. Oceanogr.* **26:**307–355.
Ndiaye, I. (2013) Etude de la biologie de la sardinelle ronde *Sardinella aurita* Valenciennes, 1847 de la zone côtière sénégalaise : Reproduction et Croissance. Mémoire de fin d'étude, Dakar: Univ. Cheikh Anta Diop.
Ospina-Alvarez, A., Parada, C. and Palomera, I. (2012) Vertical migration effects on the dispersion and recruitment of european anchovy larvae: from spawning to nursery areas. *Ecol. Model.* **231:**65–79.
Peliz, A., Marchesiello, P., Dubert, J. *et al.* (2007) A study of crab larvae dispersal on the western iberian shelf: physical processes. *J. Mar. Syst.* **68:**215–236.
Penven, P., Roy, C., COLIN de VERDIÈRE, A. *et al.* (2000) Simulation of a coastal jet retention process using a barotropic model. *Oceanologica Acta 23* **61:**5–634.
Penven, P., Echevin, V., Pasapera, J. *et al.* (2005) Average circulation, seasonal cycle, and mesoscale dynamics of the peru current system: a modeling approach. *J. Geophys. Res.* **110:**c10, C10021.
Penven, P., Marchesiello, P., Debreu, L. *et al.* (2008) Software tools for pre- and post-processing of oceanic regional simulations. *Environ. Model. Softw.* **23:**660–662.
Perry, R.I., Cury, P., Brander, K. *et al.* (2010) Sensitivity of marine systems to climate and fishing: concepts, issues and management responses. *J. Mar. Syst.* **79:**427–435.
Rebert, J.P. and Prive, M. (1974) Observation de courant sur le plateau continental sénégalais du Cap Vert au Cap ROXO, mars 1974. *Cent. Rech. ocganogr. Dakar, Arch.* No 4. 25pp.
Risien, C.M. and Chelton, D.B. (2008) A global climatology of surface wind and wind stress fields from eight years of QuikSCAT scatterometer data. *J. Phys. Oceanogr.* **38:**2379–2413.
Roy, C. (1992) Réponses des stocks de poissons pélagiques à la dynamique des upwellings en Afrique de l'Ouest: analyse et modélisation. Etudes et Thèses, ORSTOM, Paris. 146 pp.
Roy, C. (1998) An upwelling-induced retention area off Senegal: a mechanism to link upwelling and retention processes. *South Afr. J. Mar. Sci.* **19:**89–98.
Salat, J. and Cruzado, A. (1981) Masses D'eau Dans La Mediterranée Occidentale: Mer Catalane et Eaux Adjacentes. *Rapports et Proces-Verbaux Des Reunions-Commission Internationale Pour l'Exploration Scientifique de La Mer Mediterranée (CIESM). V.27 (6).*
Santos, A., Miguel, P., Alexander , S. *et al.* (2005) Decadal changes in the canary upwelling system as revealed by satellite observations: their impact on productivity. *J. Mar. Res.* **63:**359–379.
SCOR Working Group (1975) Coastal upwelling processes. *CUEA Newslett.* **4:**12–20.
Shchepetkin, A.F. and McWilliams, J.C. (2005) The Regional Oceanic Modeling System (ROMS): a split-explicit, free-surface, topography-following-coordinate oceanic model. *Ocean Model.* **9:**347–404.
Smith, W.H.F. and Sandwell, D.T. (1997) Global sea floor topography from satellite altimetry and ship depth soundings. *Science* **277:**1956–1962.
Stramma, L., Hüttl, S. and Schafstall, J. (2005) Water masses and currents in the upper tropical Northeast Atlantic off Northwest Africa. *J. Geophys. Res.* **110:**C12, C12006.
Taleb, O.S.M. (2005) Les ressources de petits pélagiques en Mauritanie et dans la zone nord ouest africaine: variabilité spatiale et temporelle, dynamique et diagnostic. PhD, Agrocampus Rennes Pôle Halieutique, Rennes.
Troupin, C., Machin, F., Ouberdous, M. *et al.* (2010) High-resolution climatology of the northeast atlantic using Data-Interpolating Variational Analysis (DIVA). *J. Geophys. Res.* **115:**C005512.
Van Camp, L., Nykjaer, L., Mittelstaedt, E. *et al.* (1991) Upwelling and boundary circulation off northwest Africa as depicted by infrared and visible satellite observations. *Prog. Oceanogr.* **26:**357–402.
Wooster, W.S., Bakun, A. and McLain, D.R. (1976) The seasonal upwelling cycle along the eastern boundary of the North Atlantic. *J. Mar. Res.* **34:**130–141.

SUPPORTING INFORMATION

Additional Supporting Information may be found in the online version of this article:

Figure S1. Bathymetry maps from the SM1 (left), SM2 (middle) model configurations and Gebco (right) observations.

Figure S2. Bathymetry spatial profiles for (a) SM1 (left) and SM2 (right) solutions. The 60m-isobath (black line) and the 200m-isobath (red line) are represented for the inner and the outer shelf respectively.